Supplement of Atmos. Chem. Phys., 23, 375–388, 2023
https://doi.org/10.5194/acp-23-375-2023-supplement

Atmospheric Chemistry and Physics
Open Access
EGU

Supplement of

Capturing synoptic-scale variations in surface aerosol pollution using deep learning with meteorological data

Jin Feng et al.

Correspondence to: Jin Feng (jfeng@ium.cn)

Supplement

1. Formula

Formulas of ventilation potency, vertical diffusion potency, and wet deposition potency of aerosols.

The original formula of ventilation potency is complex (Feng et al., 2018). Here we use a simplified version that only contains 10-m and 100-m wind speeds as

$$\text{ventilation potency} = \left(\sum_{ground}^{100m} wind\ speed\right)^{-0.25}. \quad \text{(S1)}$$

The vertical diffusion potency is denoted as PBLH^{-1}. And the wet deposition potency is

$$\text{wet deposition potency} = e^{[1-\delta(r)]}, \quad \text{(S2)}$$

where where r is the daily mean accumulated precipitation rate (mm day^{-1}), and

$$\delta(r) = \begin{cases} 1, & r \geq 3 \\ 0, & r < 3 \end{cases}, \quad \text{(S3)}$$

2. Table

Table S1 Input variable groups for sensitivity experiments.

Group name	variables
near-surface wind	10-m wind components, 100-m wind components, ventilation potency, max. 100-m wind speed
near-surface temperature-humidity	2-m temperature, 2-m mixing ratio, 2-m potential temperature, 2-m wet-equivalent potential temperature, max. 2-m temperature
near-surface vertical diffusion	surface turbulence stress components, vertical diffusion potency, max. and min. low troposphere stability
spatiotemporal geographic	Population density, high vegetation cover, Surface altitude, Latitude and Longitude, Day of year
synoptic pattern and radiation	surface pressure, downward shortwave radiation, low cloud cover, geopotential height at 850 hPa, temperature at 850 hPa
precipitation	precipitation, wet-deposition potency

3. Figure

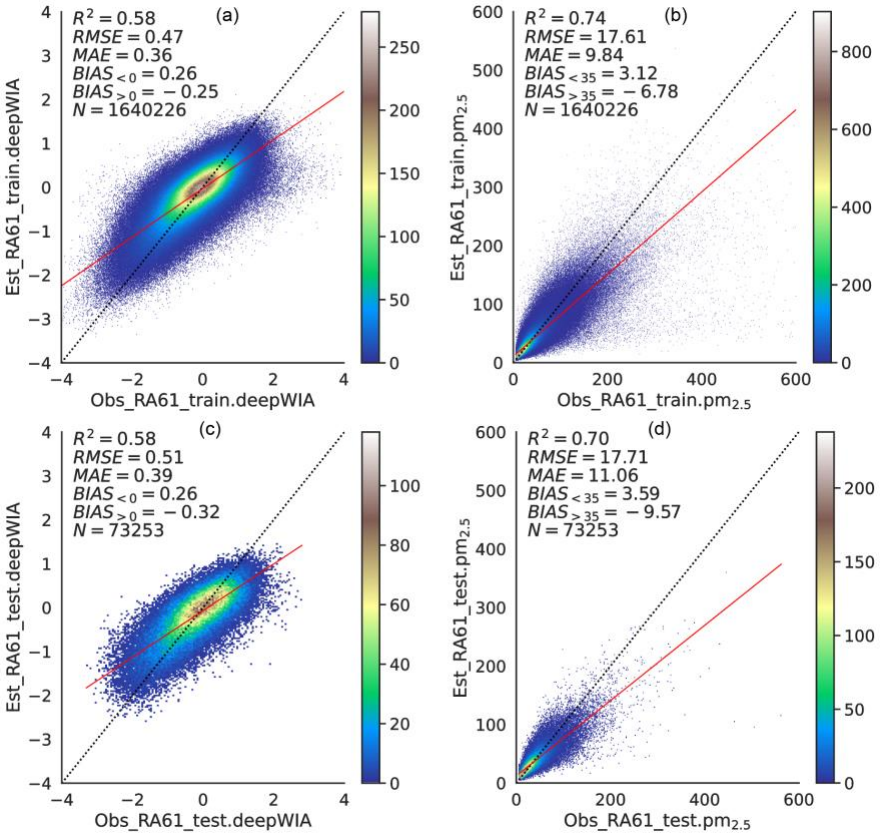

Fig S1. Fitting scatterplots of (a, c) $\hat{r}$ and (b, d) $PM_{2.5}$ concentrations for the (a, b) training and (c, d) test dataset using the 61-day running average as the background. Noted that sizes of the training and test dataset are smaller than that of the original deepWIA model because of the longer timescale of rolling average. The model performance is close to the original one on both the training dataset (Fig. 3) and test dataset (Fig. 5).

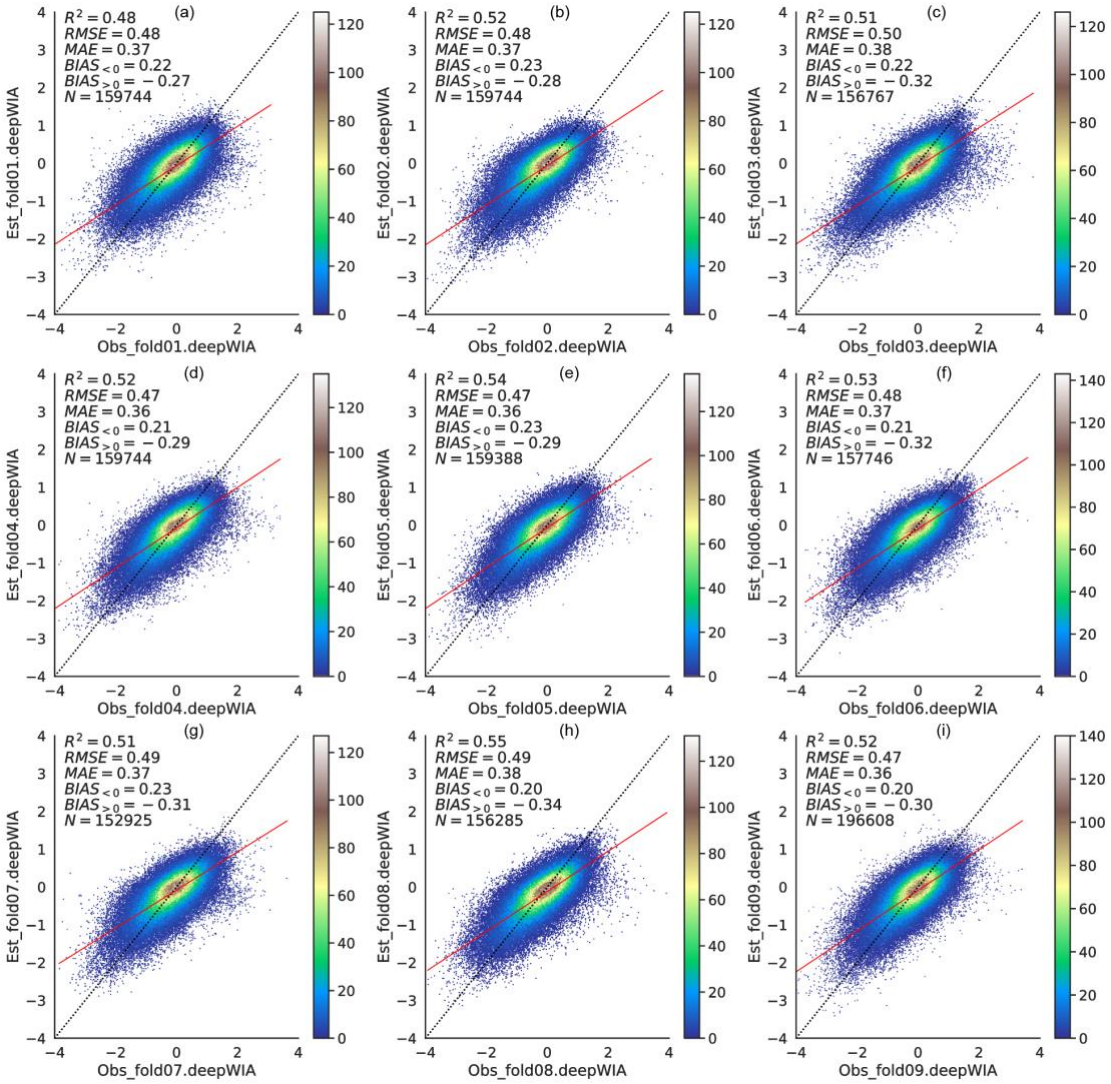

Fig S2. Same as Fig 4 (a) but for other nine validation sets.

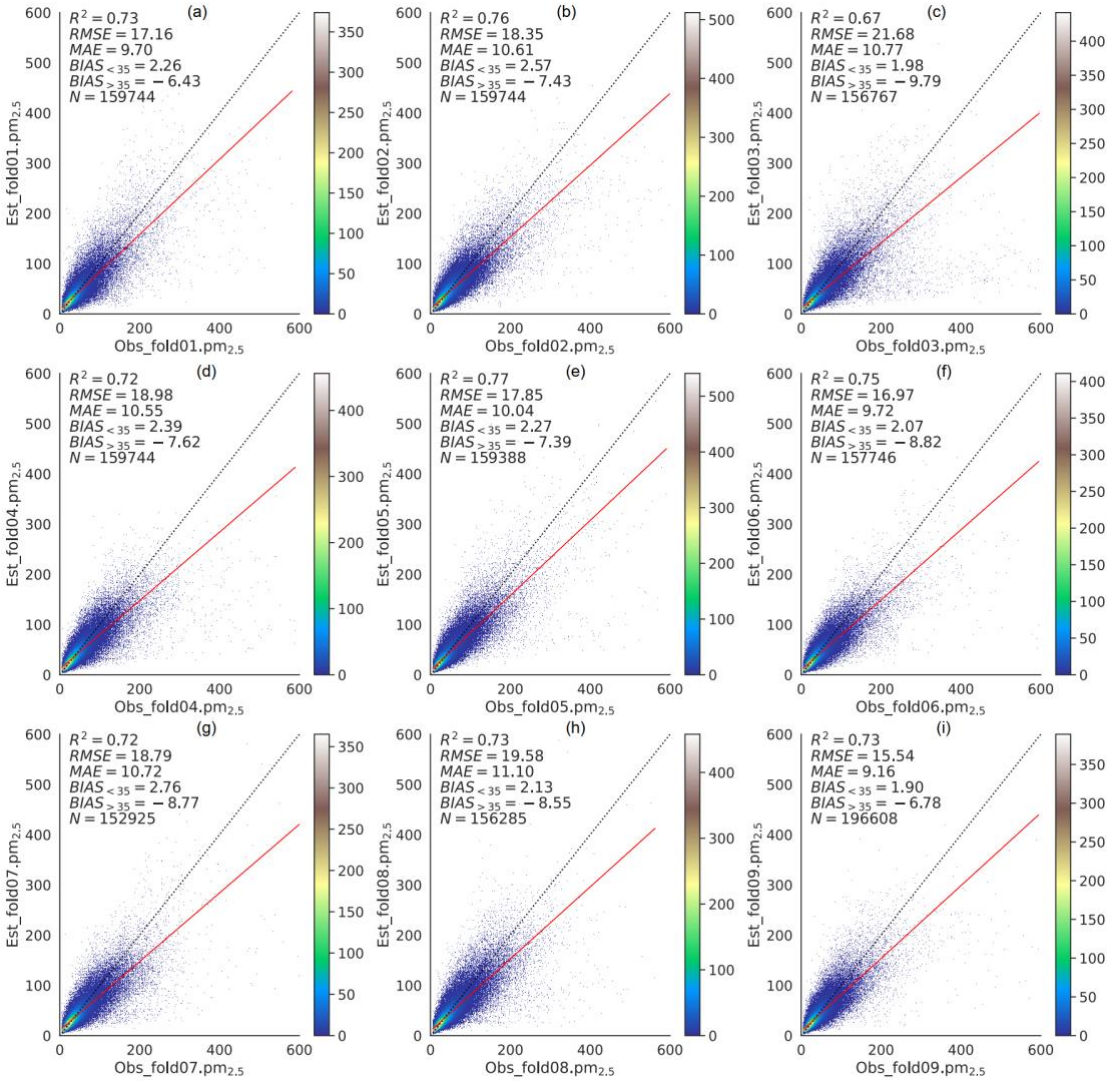

Fig S3. Same as Fig 4 (b) but for other nine validation sets.

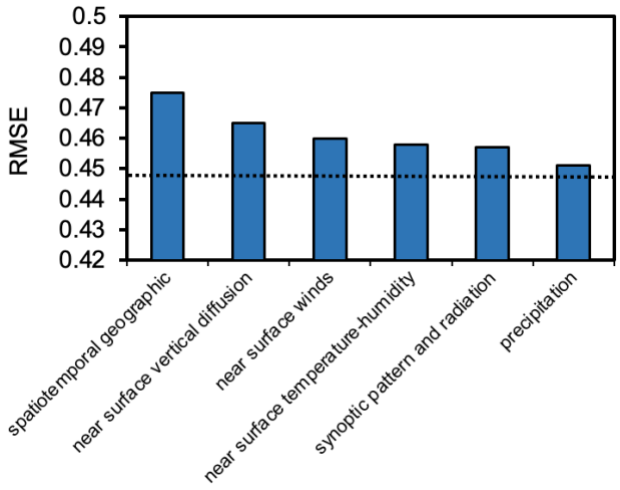

Fig S4. RMSEs of the deepWIA models on training set when the corresponding variable groups (Table S1) are not activated. Dotted line indicates the RMSE of the original deepWIA model.

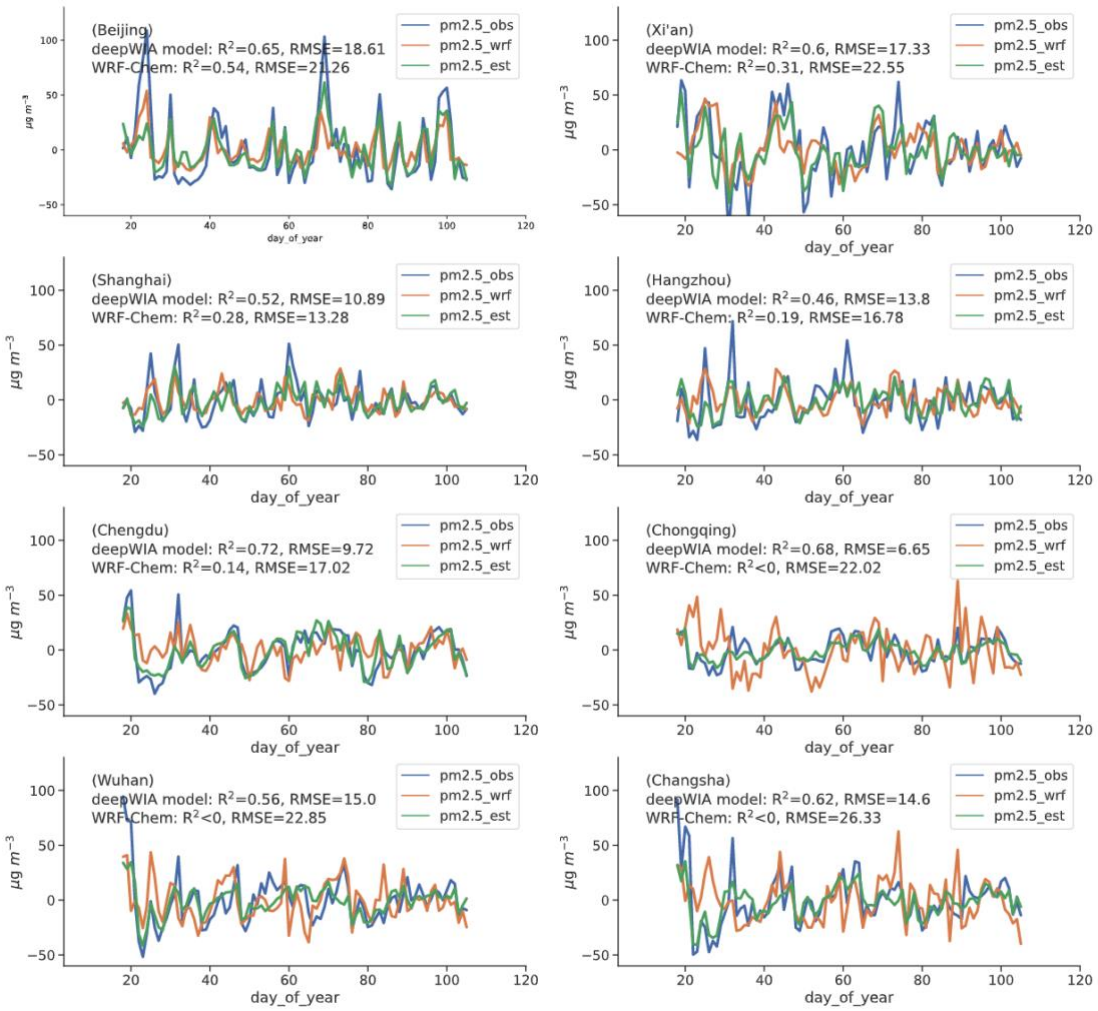

Fig S5. Same as Fig 7 but for 31-day running averaged curves. Values for the beginning and end 15 days of the test period are not included due to the running average.

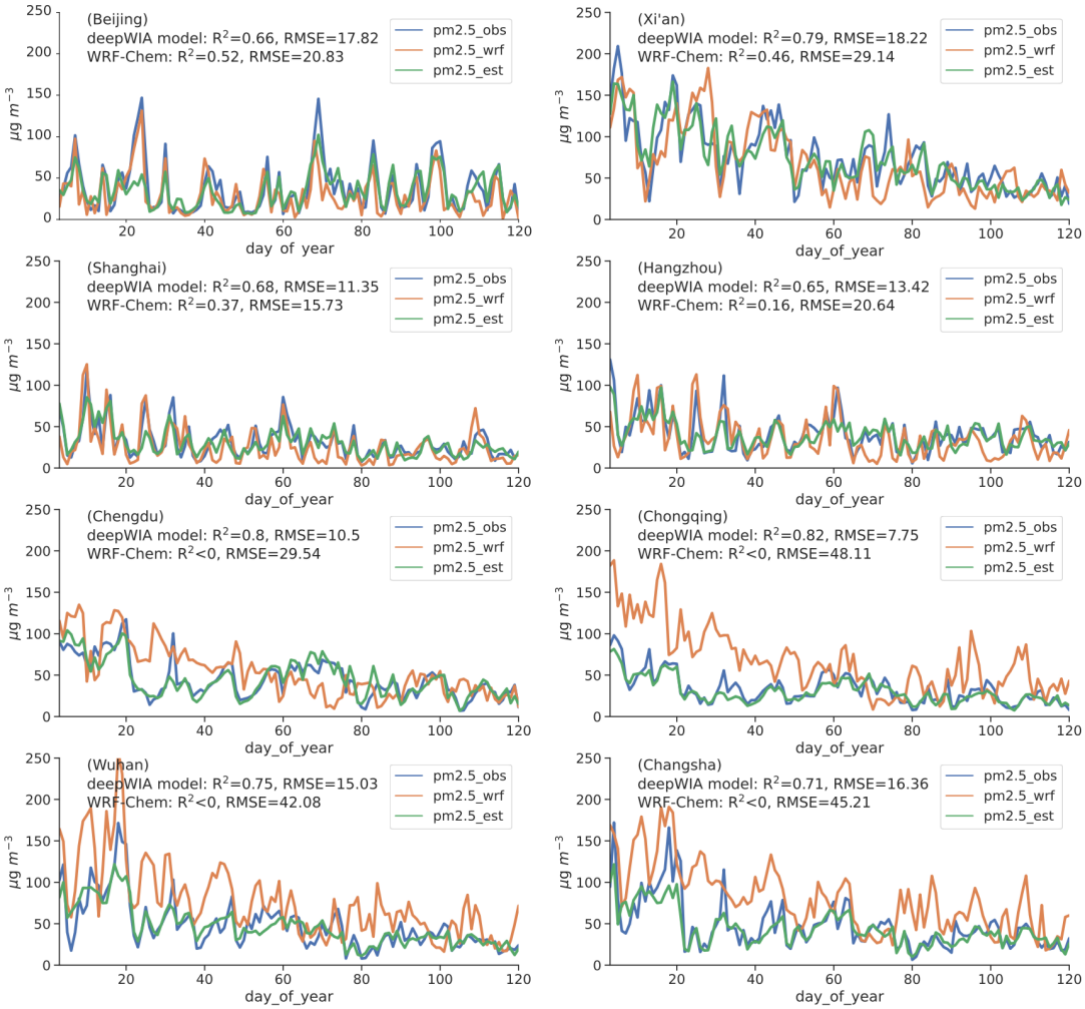

Fig S6. Same as Fig 7 but using the operational regional air quality forecast system based on WRF-Chem. The 3D-Var assimilation (Sun et al., 2020) is included in the system.

References:

Feng, J., Quan, J., Liao, H., Li, Y., and Zhao, X.: An Air Stagnation Index to Qualify Extreme Haze Events in Northern China, Journal of the Atmospheric Sciences, 75, 3489–3505, https://doi.org/10.1175/JAS-D-17-0354.1, 2018.

Sun, W., Liu, Z., Chen, D., Zhao, P., and Chen, M.: Development and application of the WRFDA-Chem three-dimensional variational (3DVAR) system: aiming to improve air quality forecasting and diagnose model deficiencies, Atmospheric Chemistry and Physics, 20, 9311–9329, https://doi.org/10.5194/acp-20-9311-2020, 2020.